Magnetic properties of Co/Re hcp$(10\bar{1}0)$ superlattices

T. Charlton, J. McChesney, and D. Lederman
Physics Department, West Virginia University, Morgantown, West Virginia 26506-6315

F. Zhang, J. Zachary Hilt, and Michael J. Pechan
Physics Department, Miami University, Oxford, Ohio 45056

(Received 4 September 1998; revised manuscript received 14 December 1998)

hcp$(10\bar{1}0)$ Co/Re superlattices were grown via magnetron sputtering on $Al_2O_3(11\bar{2}0)$ substrates. The thickness of the Co layers was approximately 1.8 nm with the Re layer thickness varying between 0.5 nm and 3.0 nm. Low angle x-ray reflectivity revealed that for our growth conditions the interfacial roughness is approximately 0.4 nm in each material at each interface. High angle x-ray diffraction, together with off-specular x-ray diffraction, showed that the growth is epitaxial with the [0001] axis in-plane and parallel to the Al_2O_3[0001] axis. Magnetization measurements indicate the presence of an in-plane uniaxial anisotropy in all samples and antiferromagnetic coupling when the Re layer thicknesses are less than 1.0 nm and close to 2.0 nm. The uniaxial anisotropy was measured via ferromagnetic resonance and determined to be approximately 5 times smaller than in bulk Co for thicker Re layer samples. For thin Re samples, a spin-flop transition causes a competition between the anisotropic magnetoresistance and the giant magnetoresistance when the external field is applied parallel to the easy axis. The most notable consequence is that the magnetoresistance is positive for small fields and negative for large fields when the current is perpendicular to the applied field. We also report a magnetoresistance of $\sim$4.5% at 10 K, more than twice the maximum value previously reported for hcp(0001) Co/Re multilayers. Co/Re hcp$(10\bar{1}0)$ superlattices provide a new system whereby the role of in-plane magnetic anisotropy in the magnetoresistance of metallic superlattices can be studied.
[S0163-1829(99)00317-3]

I. INTRODUCTION

The phenomenon of giant magnetoresistance (GMR) has been extensively studied since its discovery[1] because of its applications in magnetic sensor technology. In trilayers and multilayers, this phenomenon relies upon the antiferromagnetic coupling between ferromagnetic layers separated by nonmagnetic metallic layers.[2] Systems that have been studied thoroughly in both trilayer and multilayer form include Fe/Cr, Co/Ag, Co/Ru, Co/Cr, and Co/Cu combinations.[3,4] A system that has not received as much attention is the Co/Re system. The largest GMR reported for Co/Re multilayers to date does not exceed 2% at 18 K.[5] In all of the past studies of Co/Re multilayers, the samples were hcp[0001]-oriented with no indication of in-plane epitaxy.[5,6]

There is much interest in the interplay between strong uniaxial in-plane anisotropies and antiferromagnetic coupling between layers because the anisotropy can stabilize the domain structure in the material, significantly alter the GMR behavior, and provide knowledge about fundamental magnetic interactions. The unusual magnetic and transport properties that this combination causes have been studied in Fe/Cr(211) superlattices,[7] Co/Cr multilayers,[8–11] and Co/Ir multilayers.[12] From a fundamental point of view, these systems can also be used to study spin-flop transitions in antiferromagnets, as was previously done in Co/Cr(211) superlattices.[13]

In this work, we study the growth and magnetic properties of Co/Re superlattices grown on $Al_2O_3(11\bar{2}0)$ along the hcp$[10\bar{1}0]$ direction. The samples were grown via magnetron sputtering with the Co layer thickness fixed at $\sim$1.8 nm with varying Re layer thicknesses. The samples are epitaxial, with their *c* axis in the plane of the film. As a result, the superlattices have a significant in-plane twofold magnetic anisotropy which depends on the Re layer thickness. Antiferromagnetic coupling is evident for Re layer thicknesses below 1.0 nm from magnetization and magnetotransport measurements. Interestingly, the magnetotransport in these samples is a combination of GMR, which depends on spin-dependent electron interface scattering, and anisotropic magnetoresistance (AMR), which depends on the direction of the magnetization with respect to the applied current. Depending on the direction of the *c* axis and the applied current with respect to the external magnetic field, the GMR and AMR can have opposite signs and compete with each other, while in other instances they can reinforce each other. This results in unusual magnetotransport properties. The maximum magnetoresistance at 10 K is $\sim$4.5%, a factor of two larger than previous work on Co/Re multilayers. We also discovered that antiferromagnetic coupling occurs for other Re thicknesses, although the GMR is very small or negligible because of the large magnetic anisotropy with respect to the antiferromagnetic coupling constant.

II. EXPERIMENTAL PROCEDURES

A. Growth

The samples were grown at West Virginia University via magnetron sputtering in a high vacuum system with a base pressure of 3.0×10^{-7} Torr. The system consists of four

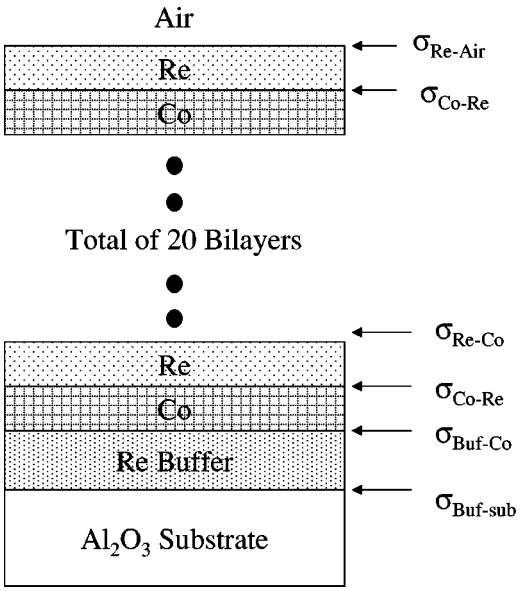

FIG. 1. Sketch of the superlattice structure used in this paper. σ is the roughness corresponding to each interface.

sputtering guns in a cluster focused on the substrate, with each gun having a shutter controlled by a crystal monitor controller. Each of the Co and Re sputtering sources has its own quartz crystal monitor. The crystal monitors were calibrated by depositing a thin film on a glass substrate and then determining its thickness from the interference pattern of the low-angle x-ray reflectivity. Up to five substrates can be mounted inside the chamber at one time. A quartz lamp heater can heat up the surface of the substrate to 575 °C, which was calibrated with respect to the heater's thermometer by placing a thermocouple sensor on a substrate's surface.

The $Al_2O_3(11\bar{2}0)$ substrates were etched in a phosphoric and sulfuric acid 3:1 mixture at 140 °C prior to mounting in the chamber. After the chamber achieved its base pressure, the substrate was heated to 575 °C for 15 min to further clean its surface. The substrate's temperature was then reduced to 560 °C, and a nominally 5.0 nm thick buffer layer of Re was grown. This temperature was chosen because low angle and high angle x-ray diffraction showed that it yielded the smoothest, most crystalline Re buffer layers. In-plane x-ray diffraction revealed that this layer grew along the hcp$[10\bar{1}0]$ direction and was epitaxial, with the [0001] direction of the Re coinciding with that of the Al_2O_3. The superlattices used to measure the magnetoresistance were grown on the buffer layer at a temperature of 158 °C (see Sec. III below). A total of twenty superlattice periods were deposited, with the Co layer being deposited first on the buffer layer. A sketch of the superlattice structure is found in Fig. 1.

B. X-ray diffraction

The structure of the multilayers was analyzed using both small and high angle x-ray diffraction at West Virginia University. The data were acquired using a Cu rotating anode source attached to a bent graphite crystal monochromator optimized for K_α radiation, and a four-circle, 29 cm base goniometer. For the low angle scans, the width of the incoming beam was approximately 0.02°. The slits in front of the detector were set to an angular width of 0.12° in order to admit all of the specular intensity for all the angles of interest. The low angle x-ray reflectivity was measured by performing a $\theta-2\theta$ scan at the specular condition, and then scanning again with θ offset by 0.10° to determine the diffuse background. The diffuse background was subtracted from the specular scan to obtain the true specular reflectivity.[14] The true specular reflectivity was modeled using an optical reflectivity model[15] from which the interfacial roughness was determined.

High angle x-ray diffraction was performed on the same goniometer described above, but the incoming beam was collimated by slits to approximately 0.20° wide, while the detector slits were set to an angular width of 0.08°. Some $\theta-2\theta$ scans were performed with the wave vector $\boldsymbol{q}$ along the growth direction while others were performed with $\boldsymbol{q}$ having a component perpendicular to the growth direction. The latter in-plane scans were used to determine the structural in-plane coherence. ϕ scans of the in-plane peaks were also performed by rotating the sample about the growth direction while the detector was fixed at the Bragg condition of the in-plane peak. The appearance of discrete peaks in a ϕ scan, corresponding to the crystal symmetry of the film, indicates that the sample is epitaxial. This technique has been previously used to determine the epitaxy of Fe/Rh and Fe/V superlattices, among others.[16,17]

C. Magnetization measurements

A commercial superconducting quantum interference device (SQUID) magnetometer at West Virginia University was used to measure the absolute saturation volume magnetization of the samples at room temperature. The angular dependence of the magnetization hysteresis loops were carried out using a vibrating sample magnetometer (VSM) at Miami University and at West Virginia University using a conventional dc magneto-optic Kerr effect (MOKE) technique at room temperature.[18] All samples were cut to very nearly the same shape ($\sim 3\times 3$ mm^2 squares) to minimize geometry effects in the measurements. Sample volumes of the Co layers were obtained using the deposited thickness, obtained from the fit of the true specular x-ray reflectivity, and the area, determined by scanning the image into a computer and calculating the area with a drawing program. The area of the samples was also measured with a caliper.

D. Ferromagnetic resonance

FMR measurements were made at room temperature with the external magnetic field in the plane of the sample. The sample was mounted in a 35 GHz cavity, film side down, at the bottom of the cavity. Angle-dependent data were obtained by rotating the magnet about the cavity. Multiple peaks in a given spectra were resolved using a spectral fitting program if necessary. The effective magnetization and anisotropy of the sample was determined by fitting the line position as a function of angle to the resonance equation of a flat disk with the external field applied in the plane of the sample.[19] The resonance equation is given by

$$\left(\frac{\omega_0}{\gamma}\right)^2 = [H\cos(\phi-\phi_H)+4\pi M_{\text{eff}} + (H_{A1}+2H_{A2})\cos^2\phi - 2H_{A2}\cos^4\phi] \times [H\cos(\phi-\phi_H)+(H_{A1}+H_{A2})\cos(2\phi) - H_{A2}\cos(4\phi)], \quad (1)$$

where ω_0 is the frequency of the source (35 Ghz), ϕ and ϕ_H are the angles of the magnetization M and the applied field H, respectively, with respect to the c axis, $\gamma = g\mu_B/\hbar$ is the gyromagnetic ratio, g is the g factor for Co ($g=2.19$), M_{eff} is the effective magnetization obtained from the analysis, and H_{A1} and H_{A2} first- and second-order anisotropy fields. At 35 GHz ϕ and ϕ_H are essentially equal. The anisotropy fields are described by $H_{Ai}=2K_i/M_{\text{sat}}$, where K_1 and K_2 are the first- and second-order anisotropy constants of a uniaxial anisotropy energy of the form $U_K=K_1\sin^2\phi+K_2\sin^4\phi$, and M_{sat} is the saturation magnetization measured by SQUID magnetometry. Any possible out-of-plane uniaxial anisotropy is included in M_{eff}.

E. Magnetotransport measurements

The magnetoresistance of the samples was measured using the standard dc four-point Van der Pauw technique in a 5.5 T superconducting magnet at a temperature of 10 K. The measurements were carried out in the following configurations: (1) $H\|c$, $H\perp I$; (2) $H\|c$, $H\|I$; (3) $H\perp c$, $H\|I$; and (4) $H\perp c$, $H\perp I$. Here c represents the direction of the (in-plane) c axis, and I the direction of the applied current. The data were acquired by scanning the magnetic field from positive to negative values.

III. RESULTS AND DISCUSSION

A. Structure

All of the samples used in the present study had similar interface roughness characteristics, according to our x-ray fits. Figure 2 shows the x-ray reflectivity data and the fit for two of these samples. The solid lines in the graphs represent fits to the model mentioned above.[15] The interface roughness between the Co and Re layers is $\sigma\sim 0.4$ nm± 0.2 nm, where 2σ is approximately the full ''width'' of the interface. The uncertainty of these numbers was determined by changing the roughness parameters by hand and then obtaining a χ^2 value after fitting all other parameters. χ^2 was then plotted as a function of the roughness parameter in order to determine the sensitivity of the model to the parameter. Other important parameters that were obtained include the average Co and Re layer thicknesses, the Re buffer layer thickness, and the interface roughness at the top of the sample, between the buffer layer and the superlattice, and between the buffer layer and the substrate. The full results are shown in Table I.

Prior to the growth of the samples presented in this study, several superlattices with nominally identical Co and Re thicknesses ($t_{\text{Re}}=2.0$ nm, $t_{\text{Co}}=1.0$ nm) were grown at different temperatures to optimize the growth temperature. The inset of Fig. 2 shows the interface roughness parameters obtained from the fits as a function of the growth temperature. While the analysis of the specular reflectivity cannot differentiate between interdiffusion and step disorder, it is reason-

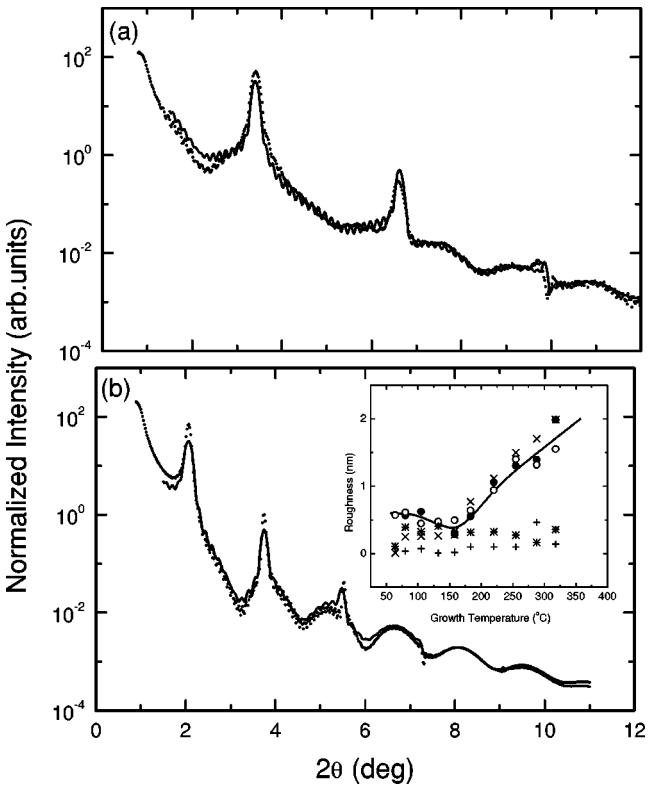

FIG. 2. Low angle x-ray true specular reflectivity for two Co/Re superlattices. The solid lines represent fits to the model described in the text and the dots represent data. For (a), the model indicates $t_{\text{Co}}=1.73$ nm, $t_{\text{Re}}=0.79$ nm, and for (b) $t_{\text{Co}}=1.87$ nm, $t_{\text{Re}}=3.03$ nm. The roughness parameters for these and the other samples can be found in Table I. Inset: Roughness parameters for nominally identical layer thicknesses ($t_{\text{Re}}=2.0$ nm, $t_{\text{Co}}=1.0$ nm) as a function of sample growth temperature. ($\times$) represents $\sigma_{\text{Re-Air}}$, ($\bullet$) represents $\sigma_{\text{Co-Re}}$, ($\circ$) represents $\sigma_{\text{Re-Co}}$, (*) represents $\sigma_{\text{Buf-Co}}$, and (+) represents $\sigma_{\text{Buf-Sub}}$. The solid line is a guide to the eye.

TABLE I. Results of fits to low angle x-ray specular reflectivity measurements. Units are in nm. Uncertainties are approximately ± 0.2 nm for roughness parameters σ and ± 0.15 nm for layer thicknesses t. For the definitions of the roughness parameters, see Fig. 1.

t_{Re}	t_{Co}	$\sigma_{\text{Buf-Sub}}$	$\sigma_{\text{Buf-Co}}$	$\sigma_{\text{Co-Re}}$	$\sigma_{\text{Re-Co}}$	$\sigma_{\text{Re-air}}$
0.57	1.82	0.04	0.19	0.50	0.37	0.43
0.79	1.73	0.07	0.24	0.33	0.39	0.91
0.82	1.87	0.11	0.28	0.37	0.47	0.84
1.01	1.91	0.09	0.23	0.42	0.35	0.45
1.27	1.84	0.09	0.23	0.50	0.54	0.94
1.46	1.78	0.12	0.23	0.35	0.40	0.21
1.61	1.62	0.18	0.25	0.30	0.42	0.19
1.73	1.86	0.01	0.19	0.40	0.33	0.22
1.89	1.87	0.11	0.39	0.58	0.32	0.32
2.11	1.82	0.12	0.25	0.39	0.44	0.40
2.37	1.77	0.16	0.26	0.51	0.45	0.64
2.50	1.79	0.07	0.23	0.44	0.67	0.30
3.03	1.87	0.12	0.30	0.53	0.69	0.76

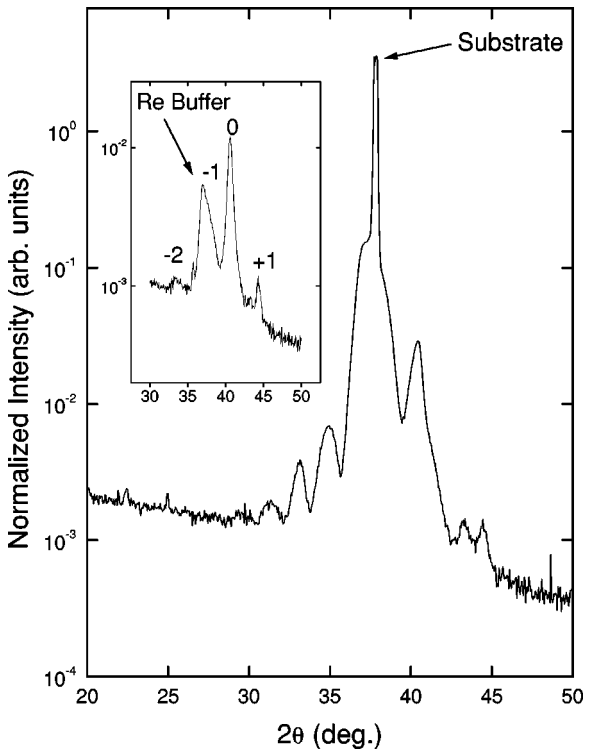

FIG. 3. High angle $\theta-2\theta$ scan with $\boldsymbol{q}$ along the growth direction for the $t_{Re}=0.79$ nm sample. The Al_2O_3 substrate's $(11\bar{2}0)$ peak is indicated. Inset: $\theta-2\theta$ scan with θ misoriented by 1.07°. This lowers the intensities of the substrate peak and the Re buffer layer's finite-size peak, so that the superlattice peaks are more evident. The Re buffer layer $(10\bar{1}0)$ peak, as well as the superlattice peaks are indicated. The numbers indicate the order of the superlattice peak.

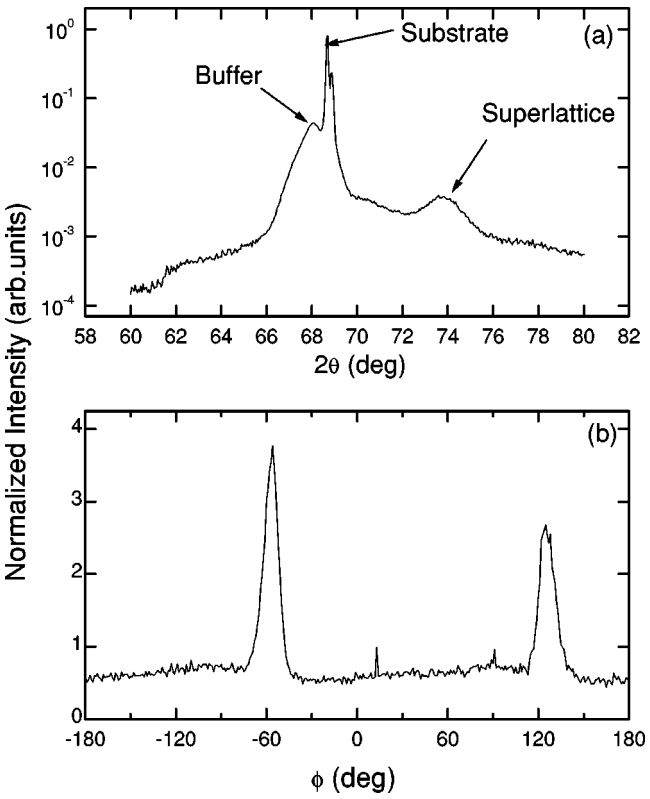

FIG. 4. (a) is a $\theta-2\theta$ scan of the $t_{Re}=0.79$ nm superlattice with $\boldsymbol{q}$ along the $[11\bar{2}0]$ direction of the buffer layer and the superlattice. The substrate $(03\bar{3}0)$, the Re buffer layer $(11\bar{2}0)$, and the superlattice equivalent $(11\bar{2}0)$ peaks are indicated. (b) is a ϕ scan obtained by rotating the sample about the superlattice $[10\bar{1}0]$ (growth) direction with $\boldsymbol{q}$ kept fixed at the superlattice $(11\bar{2}0)$ Bragg condition. The twofold in-plane crystalline symmetry of the superlattice is evident.

able to assume that at low growth temperatures the interface roughness comes about from step disorder, while at high temperatures it is dominated interdiffusion. This is possible because Co and Re form an alloy for all concentrations at high temperatures.[20] From this study, the optimal growth temperature of the superlattice was determined to be $\sim 158\,^{\circ}\mathrm{C}$.

Figure 3 shows a high angle $\theta-2\theta$ scan with the wave vector $\boldsymbol{q}$ along the growth direction of the $t_{Re}=0.79$ nm sample. The Al_2O_3 substrate $(11\bar{2}0)$ peak, the Re buffer layer's $(10\bar{1}0)$ peak, as well as the main superlattice peak are indicated. Note the fringes around the Re buffer layer peak, which result from the long-range lateral length scale smoothness of the 5.3 nm thick buffer layer (according to the low angle x-ray scattering, the rms roughness at the buffer layer-superlattice interface is only ~ 0.1 nm). The inset of Fig. 3 shows a $\theta-2\theta$ scan with θ misaligned by 1.07° with respect to $2\theta/2$. In this scan the superlattice peaks are observed more clearly because the rocking curve of the substrate is much narrower ($\sim 0.08°$) than the misalignment, and also because this technique effectively eliminates the fringe peaks resulting from the Re buffer layer. In contrast, typical rocking curve full widths at half maximum of the main superlattice peak were in the $3°-5°$ range. In this way, the main superlattice peak, as well as the satellite peaks, are clearly visible. The high angle patterns were not analyzed quantitatively because the presence of the buffer layer fringes complicated the analysis. However, it is clear from these scans that the samples are crystalline and $[10\bar{1}0]$ oriented.

Figure 4(a) is a $\theta-2\theta$ scan of the $t_{Re}=0.79$ nm superlattice with $\boldsymbol{q}$ along the $[11\bar{2}0]$ direction of the buffer layer and the superlattice, that is, with $\boldsymbol{q}$ having a component perpendicular to the growth direction. The substrate $(03\bar{3}0)$, the Re buffer layer $(11\bar{2}0)$, and the superlattice equivalent $(11\bar{2}0)$ peaks are indicated. Figure 4(b) is a ϕ scan about the superlattice $[10\bar{1}0]$ (growth) direction with $\boldsymbol{q}$ kept fixed at the superlattice $(11\bar{2}0)$ Bragg condition. The twofold symmetry, characteristic of epitaxial growth, is evident as the equivalent $(11\bar{2}0)$ and $(2\bar{1}\bar{1}0)$ planes match the direction of $\boldsymbol{q}$ for ϕ angles 180° apart from each other. A similar ϕ-scan symmetry was observed for the Re buffer layer. This proves that the sample is epitaxial, with its in-plane [0001] axis parallel to the [0001] axis of the substrate. Other samples with small $t_{Re}<2.0$ nm also displayed similar in-plane peaks. In-plane peaks for samples with larger t_{Re} were more difficult to detect because of their proximity to the substrate and buffer layer peaks.

Finally, we were also interested in determining whether the strain in the Co and Re layers depends on the Re thickness because strain could cause the effective magnetization

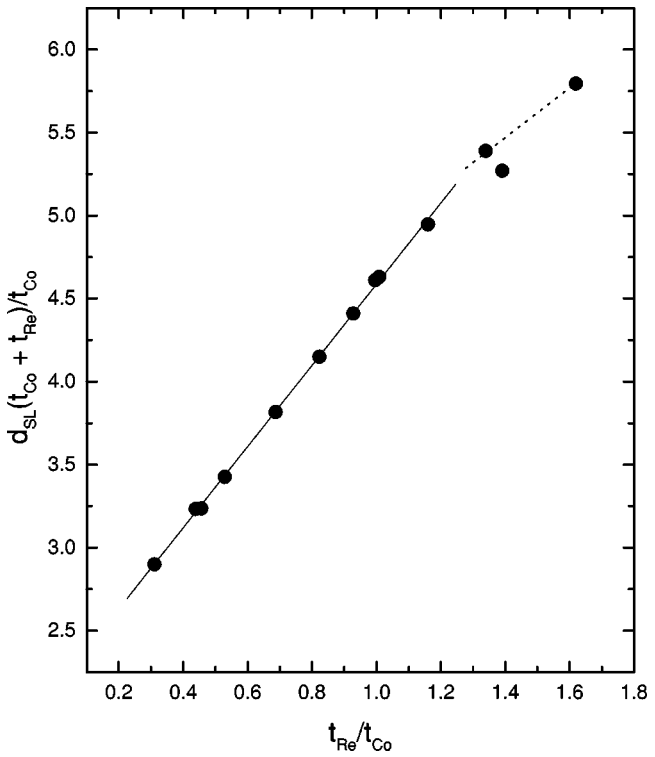

FIG. 5. $d_{SL}(t_{Co}+t_{Re})/t_{Co}$ plotted as a function of the ratio t_{Re}/t_{Co}, using the values of t_{Co} and t_{Re} obtained from the low angle x-ray reflectivity fits. The solid line represents a fit to a straight line for points with $t_{Re}/t_{Co}<1.2$, which yields interplanar distances of $d_{Re}=2.46$ nm and $d_{Co}=2.13$ nm.

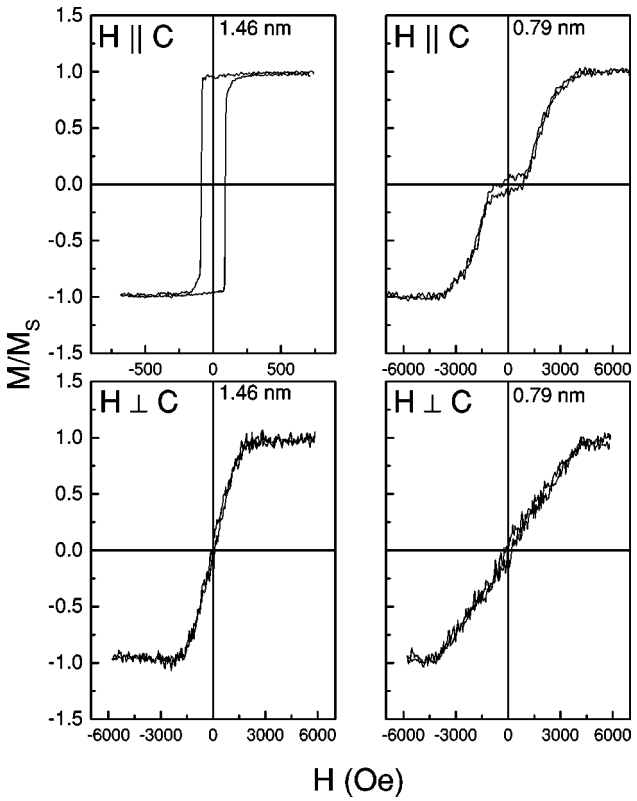

FIG. 6. Magnetization hysteresis curves measured at room temperature for two representative samples with the external magnetic field H applied both parallel and perpendicular to the Al_2O_3 $(11\bar{2}0)$ substrate's c axis. The Re layer thickness of each sample is labeled.

of the Co layers to change. If the strain were the same for all samples, then the position of the main superlattice peak would be a weighted average of the Re and Co lattice parameters:

$$d_{SL}=(t_{Co}d_{Co}+t_{Re}d_{Re})/(t_{Co}+t_{Re}), \tag{2}$$

where d_{SL} is the lattice parameter determined from Bragg's law using the position of the main superlattice peak.[21] We can rewrite this equation as

$$\frac{d_{SL}(t_{Co}+t_{Re})}{t_{Co}}=d_{Co}+d_{Re}\frac{t_{Re}}{t_{Co}}. \tag{3}$$

In Fig. 5 we have plotted $d_{SL}(t_{Co}+t_{Re})/t_{Co}$ as a function of the ratio t_{Re}/t_{Co}, using the values of t_{Co} and t_{Re} obtained from the low angle fits described above. According to Eq. (3), the graph should yield a straight line if d_{Re} and d_{Co} are the same for all samples, with the slope being d_{Re} and the intercept being d_{Co}. In Fig. 5 the straight solid line represents a linear fit for all data points with $t_{Re}/t_{Co}<1.2$. Clearly the fit is excellent, and demonstrates that the lattice parameter is on average the same for Co and Re for all samples with $t_{Re}/t_{Co}<1.2$. From the linear fit we obtain $d_{Co}=0.213$ nm and $d_{Re}=0.246$ nm, which represents an approximately 2.5% increase with respect to the Re $(10\bar{1}0)$ bulk lattice parameter of 0.239 nm, and a similar decrease of the Co lattice parameter with respect to the bulk value of 0.217 nm. This is reasonable considering that the in-plane $(1\bar{2}10)$ lattice parameter of bulk Re is 0.138 nm and that of bulk Co is 0.125 nm, so that in order to accommodate the in-plane strain, the in-plane lattice parameter of Re decreases and that of Co increases, causing the out-of-plane $(10\bar{1}0)$ lattice parameter of Re to increase and that of Co to decrease. For samples where $t_{Re}/t_{Co}>1.2$ it was difficult to identify the main superlattice peak because it was too close to the substrate and buffer layer peaks.

To summarize, a quantitative analysis of the low angle x-ray reflectivity revealed approximately 0.4 nm of interface roughness. High angle x-ray diffraction showed that the samples are oriented along the $[10\bar{1}0]$ direction with the in-plane c axis in the aligned with Al_2O_3 substrate's c axis.

B. Magnetic properties

Figure 6 shows magnetization hysteresis curves measured at room temperature for two representative samples, those with $t_{Re}=0.79$ nm and $t_{Re}=1.4$ nm, with the external magnetic field H applied both parallel and perpendicular to the Al_2O_3 $(11\bar{2}0)$ substrate's c axis. For the $t_{Re}=1.46$ nm, the loop is square with $H\|c$ and sheared with $H\perp c$. This indicates that the in-plane epitaxy indeed causes the sample to have an in-plane magnetic anisotropy. For the $t_{Re}=0.79$ nm sample, both of the curves are sheared, indicating that there is antiferromagnetic coupling between adjacent Co layers. However, note that for $H\|c$, there is a break in the slope at $H\sim1130$ Oe, whereas no break is observed with $H\perp c$. This is an indication that the magnetic anisotropy causes the antiferromagnetically-aligned Co layers to undergo a spin-flop transition, similar to the spin-flop transition in conven-

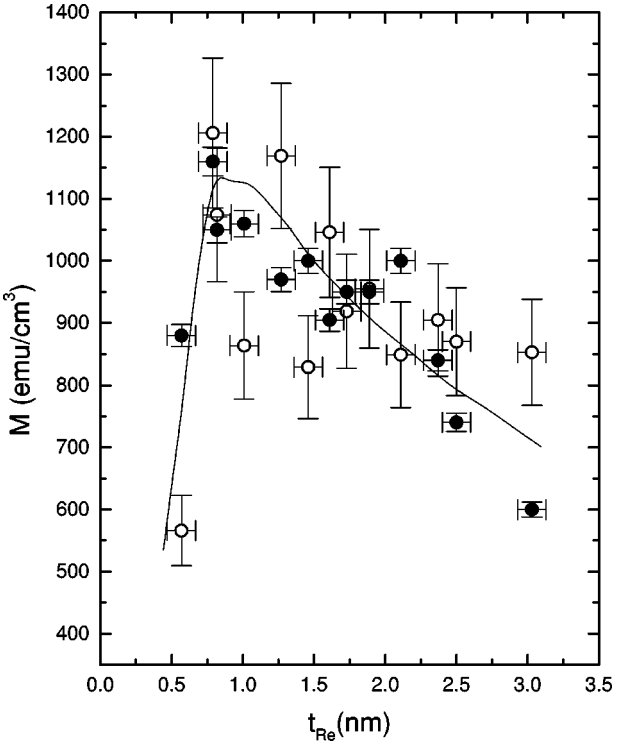

FIG. 7. Saturation magnetization M_{sat} (○), measured via SQUID magnetometry, and the effective magnetization M_{eff} (●), measured via FMR, of the Co layers at room temperature of all of the samples as a function of Re layer thickness. The uncertainty in M_{sat} ($\pm 10\%$) is a result of the uncertainty of the Co layer thickness and the sample area.

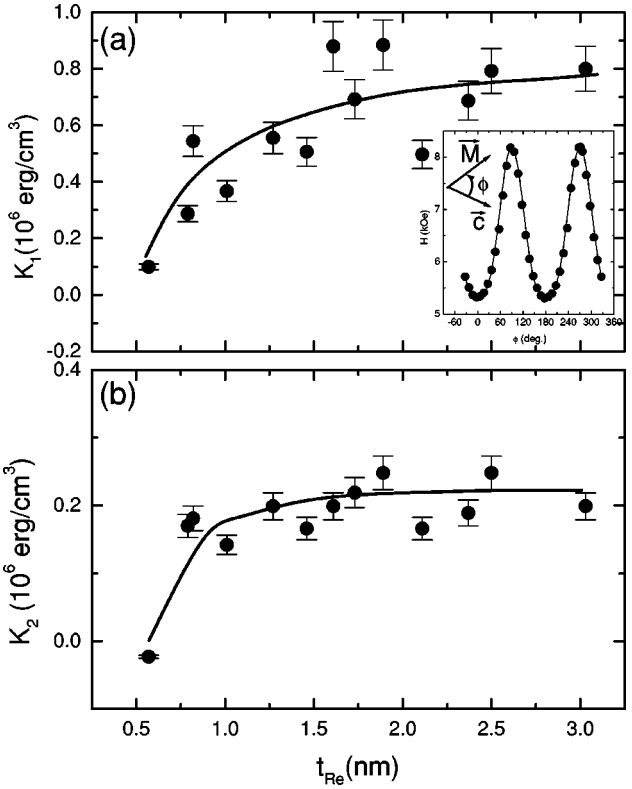

FIG. 8. (a) First order magnetic anisotropy constant K_1 and (b) second order magnetic anisotropy constant K_2 as functions of the Re layer thickness. Values were determined from FMR angular measurements. Inset: Position of the FMR line for the $t_{Re} = 1.46$ nm sample. The solid curve represents a fit to Eq. (1). The error bars are due primarily to the uncertainty in M_{sat}.

tional antiferromagnets. In conventional antiferromagnets, this transition is first order, and causes the magnetization sublattices to ''flop'' at a critical field, so that a net magnetization appears parallel to the applied field direction. The spin-flop transition in a similar Co/Re sample was recently observed directly via polarized neutron reflectivity measurements whose results will be published separately.[22] Briefly, the neutron reflectivity measured with polarization analysis of the antiferromagnetic peak was used to determine the angle of the antiferromagnetic moment as a function of magnetic field. These measurements showed that the spin-flop transition is gradual when H is applied parallel to the c axis, unlike the first-order spin-flop phase transition in conventional antiferromagnets. The effect of this behavior on the magnetoresistance measurements is discussed below.

Figure 7 shows the saturation magnetization M_{sat} of the Co layers measured at room temperature of all of the samples as a function of Re thickness. The error bars for M_{sat} represent uncertainties in the thickness of the Co layers and the sample area measurements ($\pm 10\%$). When $t_{Re} \gtrsim 1.0$ nm, M_{sat} decreases monotonically within the data uncertainty. If this trend is extended to $t_{Re} = 0$, one obtains a value of $M_{sat}(t_{Re} = 0) \sim 1400$ emu/cm^3, which agrees well with the bulk value of Co. The decrease in M_{sat} as t_{Re} increases may indicate that the Re atoms near the interfaces magnetically disorder the Co layers. One possibility is that the Re interface atoms, which suffer from some interdiffusion with the Co, may couple magnetically with a low transition temperature. Just as the Co atoms would tend to order this interfacial layer, the interfacial layer's large magnetic entropy would disorder the Co layer, thus lowering its magnetization. As the number of Re layers increases, the entropy of the boundary layer increases, thus lowering the magnetization even more. This magnetic disordering mechanism is similar to that observed in CoF_2/FeF_2 antiferromagnetic superlattices, where the Neél temperature of the FeF_2 ($T_N \sim 78.4$ K) layers is depressed by the CoF_2, which has a much lower Neél temperature ($T_N \sim 39$ K).[23] Increased strain is an unlikely source of this decrease because, as was shown above, the strain is essentially the same for all samples with $t_{Re} < 2.2$ nm. When $t_{Re} \lesssim 1.0$ nm, there is a sudden drop in M_{sat}. This drop could be due to interdiffusion, which is of the same order as the Re layer thickness in this range.

The magnetic anisotropy in these samples was obtained from FMR measurements. The inset of Fig. 8 shows the angular dependence of the position of the FMR line for the $t_{Re} = 1.46$ nm sample. The solid curve represents a fit to the model described above in Eq. (1). From similar fits to spectra obtained for every sample, we obtained values for the anisotropy constants K_1 and K_2, as well as the effective magnetization M_{eff}. M_{eff} is plotted in Fig. 7 together with M_{sat}. Note that within the experimental uncertainties in these values, M_{sat} and M_{eff} agree well in the region $t_{Re} \gtrsim 1.0$ nm. This means that there is very little, if any, surface or interface anisotropy perpendicular to the plane.

The values of K_1 and K_2 obtained from FMR are shown in Figs. 8(a) and 8(b). K_1 is small for $t_{Re} < 1.0$ nm, but eventually saturates at $\sim 0.7 \times 10^6$ erg/cm^3 as t_{Re} increases. K_2

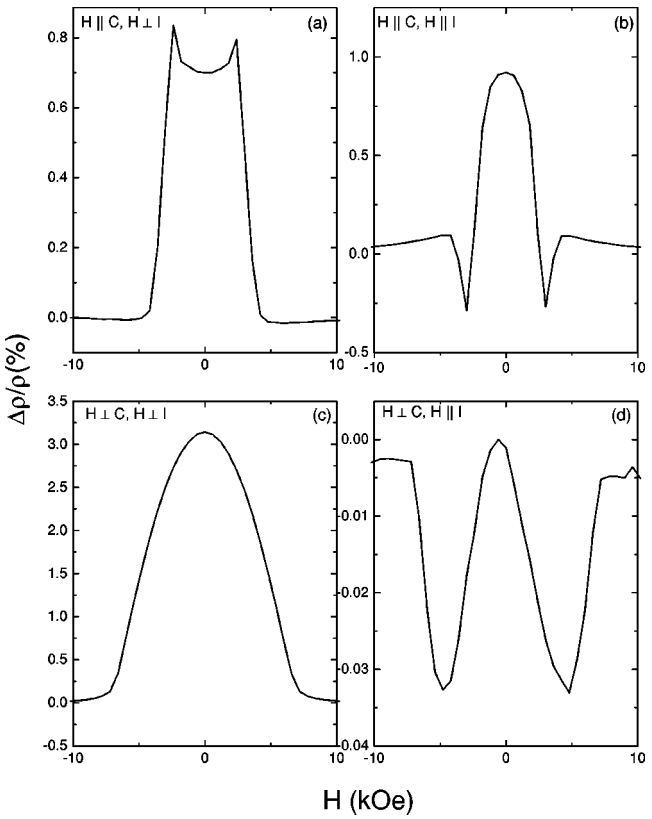

FIG. 9. Magnetoresistance measurements obtained at $T=10$ K for the $t_{Re}=0.79$ nm sample. c is the in-plane easy axis, I is the applied current, and H is the applied magnetic field.

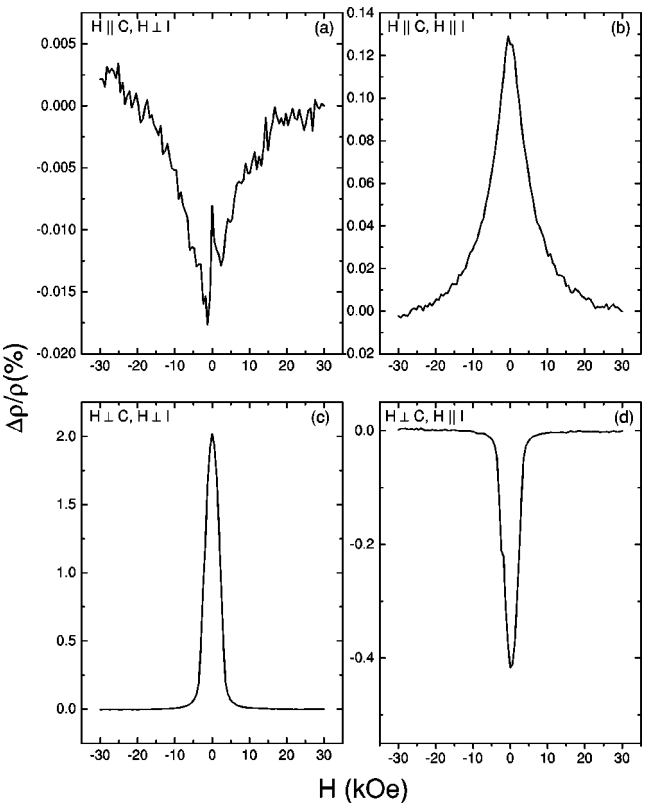

FIG. 10. Magnetoresistance measurements obtained at $T=10$ K for the $t_{Re}=1.46$ nm sample. c is the in-plane easy axis, I is the applied current, and H is the applied magnetic field.

displays a similar type of behavior, with the value saturating at $\sim 0.2\times 10^6$ erg/cm^3. For the thinnest sample K_2 is negative. This could be the result of the interface roughness, which for the thinnest sample would alter the magnetic properties of the Co layers. The values of K_1 and K_2 are lower than the room temperature values of $K_1=4.1\times 10^6$ erg/cm^3 and $K_2=1.0\times 10^6$ erg/cm^3 reported for bulk Co.[24] However, a similar reduction in the anisotropy constants has been reported for Co(10$\bar{1}$0)/Cr(211) superlattices,[25] with values of $K_1=1.8\times 10^6$ erg/cm^3 and $K_2=0.55\times 10^6$ erg/cm^3. Interestingly, the ratio for thicker Re layers $K_1/K_2\sim 3.5$ in Co/Re is similar to that obtained in 50 nm thick, *b*-axis oriented Co single films, although the actual values of the anisotropy constants in the thick films are approximately 5 times greater ($K_1=3.4\times 10^6$ erg/cm^3 and $K_2=1.0\times 10^6$ erg/cm^3).[26] This could be a result of the strain built into the Co layers, as shown in the high angle x-ray diffraction, and not due to an intrinsic effect that would alter this ratio.

Magnetoresistance (MR) measurements at 10 K for two representative samples are shown in Figs. 9 and 10. The MR is represented by $\Delta\rho/\rho\equiv(R(H)-R_S)/R_S$, where ρ is the resistivity, $R(H)$ is the resistance measured at an applied field H, and R_S is the resistance at the maximum field. The data can be qualitatively explained assuming an in-plane uniaxial anisotropy and taking into account giant magnetoresistance (GMR) and anisotropic magnetoresistance (AMR) mechanisms. The GMR relies on the increased electron scattering when the magnetization of the Co layers are antiferromagnetically aligned and is always negative, that is, it causes the electrical resistance to decrease as the field is increased from $H=0$.[4] In contrast, the AMR, which is a result of $s-d$ scattering and spin-orbit coupling,[27] depends on the direction of the magnetization M with respect to the current I. It is well known[28] that in ferromagnetic materials $\rho_\parallel>\rho_\perp$, where $\rho_\parallel$ is the resistivity measured with $M\|I$ and $\rho_\perp$ is measured with $M\perp I$. Note that if M or I are rotated by 180°, there is no change in the AMR. The maximum change in AMR occurs when M is initially either parallel or perpendicular to I and then rotates by 90°. In Co single films the AMR can be significant, on the order of a few percent, and is dependent on the film microstructure.[29] In the case of the Co/Re system, the AMR can be especially significant because the resistivity Re is approximately three times larger than that of Co (18.6 $\mu\Omega$ cm for Re vs 5.8 $\mu\Omega$ cm for Co).[30] This causes a large portion of the electron transport to occur through the Co layers, magnifying the AMR contribution.

In the $H\|c$, $H\perp I$ configuration, the $t_{Re}=0.79$ nm sample [Fig. 9(a)], which according to the magnetization measurements is antiferromagnetically coupled, shows an initial rise in the MR as H decreases from saturation to approximately 2 kOe. However, the MR decreases again as H approaches zero. This can be explained by taking into account the spin-flop transition inferred from the magnetization measurements, and corroborated by neutron diffraction. As the field decreases from saturation, the magnetizations of the Co layers change from being $M\|c$ and $M\perp I$ to being approximately $M\perp c$ and $M\|I$ near the critical field at the spin-flop transition. The degree to which M is aligned $\perp c$ near the critical field depends on the relative strengths of the mag-

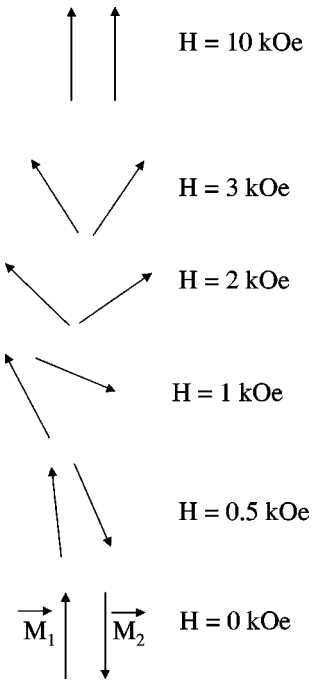

FIG. 11. Sketch of the magnetizations of adjacent cobalt layers, $\vec{M}_1$ and $\vec{M}_2$, as functions of H with $H \| c$ deduced from neutron diffraction data. Notice that the spin flop transition is gradual.

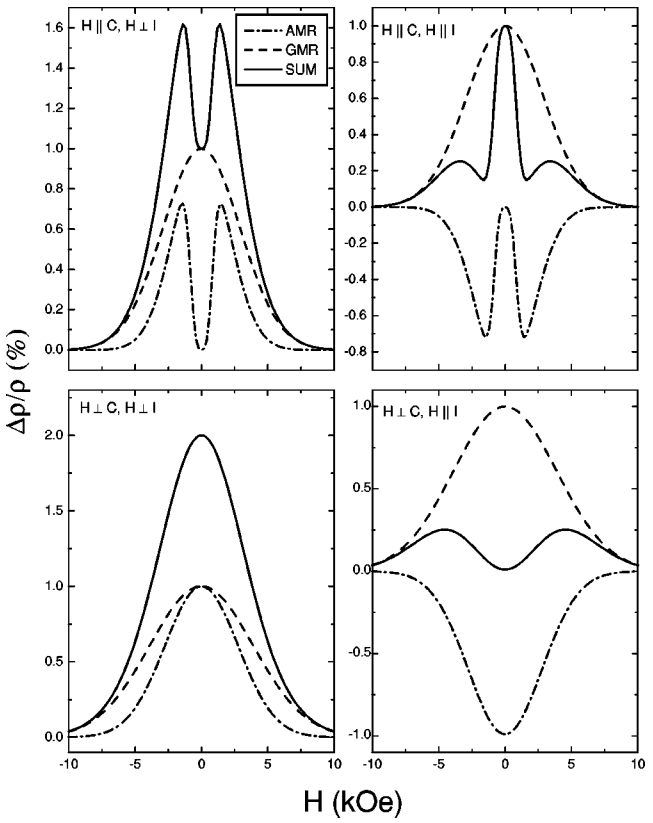

FIG. 12. Simulations of the MR data. c is the in-plane easy axis, I is the applied current, and H is the applied magnetic field. The sum of the AMR and GMR is the solid line, the AMR is the dash-dot line, and the GMR is a dashed line.

netic anisotropy and the antiferromagnetic coupling. In this region the MR increases due to the GMR, because of the change from a completely parallel to a partially antiferromagnetic alignment of the magnetizations, and due to the AMR, because the magnetizations change their direction with respect to the current. The fact that the MR peaks at 2 kOe, while the magnetization of the sample with $H \| c$ shows a change in slope at 1.1 kOe, could be a result of a nucleation of the spin-flop transition at the top and/or bottom surfaces. After the nucleation, the rest of the layers flop gradually. This causes a complicated magnetization arrangement as a function of magnetic field. This is illustrated in Fig. 11, which shows a possible spin configuration of the superlattice as a function of field. The point at which the MR peaks depends on the details of the spin orientations, because the AMR depends on the specific direction of the layer magnetizations with respect to the applied current.

Theoretical calculations by Folkerts[31] indicate that if magnetization reversal through magnetic domain wall motion, GMR is observed if $|J_{\mathrm{AF}}| > K_U t_{\mathrm{Co}}$, otherwise there is no spin-flop transition. Here J_{AF} is the antiferromagnetic coupling strength between Co layers and K_U is the effective magnetic uniaxial anisotropy constant. Following the treatment by Folkerts, the total energy per bilayer per unit area when the field is applied parallel to the easy axis can be written as

$$E = -HM(\cos\phi_1 + \cos\phi_2) - 2J_{\mathrm{AF}} t_{\mathrm{Co}} \cos(\phi_2 - \phi_1) + K_U(\sin^2\phi_1 + \sin^2\phi_2), \tag{4}$$

where ϕ_1 and ϕ_2 are the angles that the magnetizations of the two bilayers make with respect to the easy axis, H is the external field, and M is the magnetization of each Co layer. The factor of 2 in front of J_{AF} takes into account that there are two surfaces for each Co layer. Equating the expressions for the magnetic energy of the spin-flop state ($\phi_1 = \phi_2$) with the energy of the antiferromagnetic state ($\phi_1 = 0$, $\phi_2 = \pi$), one obtains an expression for J_{AF} in terms of the switching field H_{Sw}. H_{Sw} is defined as the critical field required to undergo the spin-flop transition, and is determined from the sudden change in slope in the magnetization measurements. Solving for J_{AF}, one obtains

$$J_{\mathrm{AF}} = -\frac{K_U t_{\mathrm{Co}}}{2}\left(\frac{H_{\mathrm{Sw}}^2 M^2}{4K_U^2} + 1\right). \tag{5}$$

For the $t_{\mathrm{Re}} = 0.79$ nm sample, $H_{\mathrm{Sw}} \sim 1130$ Oe from Fig. 6, $M \sim 1100$ G from SQUID measurements, and $K_U \sim K_1 + K_2 \sim 0.60 \times 10^6$ erg/cm^3 from FMR measurements. This yields $J_{\mathrm{AF}} \sim -0.11$ erg/cm^2, whose magnitude is smaller than, but of the same order of magnitude as the coupling reported for Co($1\bar{1}00$)/Cr(211) superlattices[8] (-0.24 erg/cm^2) and Fe/Cr(211) superlattices[13] (-0.55 erg/cm^2). We also calculated $J_{\mathrm{AF}} = -0.11$ erg/cm^2 from the saturation field, as was done for Fe/Cr(211) superlattices,[7] in good agreement with the calculation above. Unlike the Co/Cr(211) system, however, no separate surface and bulk-like spin-flop transitions are clearly observed in the magnetization, although separate transitions are expected because the number of bilayers is even.[13] One reason for this discrepancy could be that the J/K_U ratio in the Co/Re system is approximately 5 times smaller than in the Co/Cr(211) system, thus leading to a

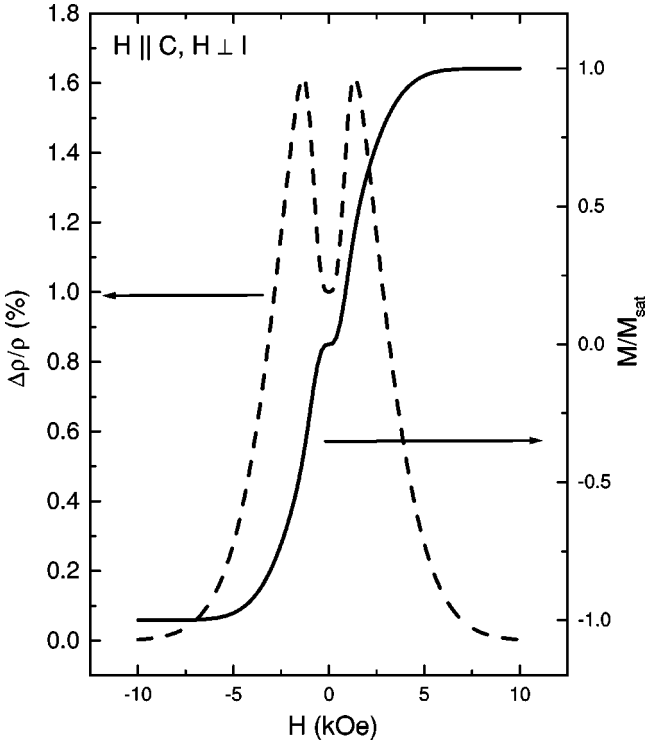

FIG. 13. Calculated MR (dashed line) and $M-H$ loop (solid line) for the $H\|c$ case.

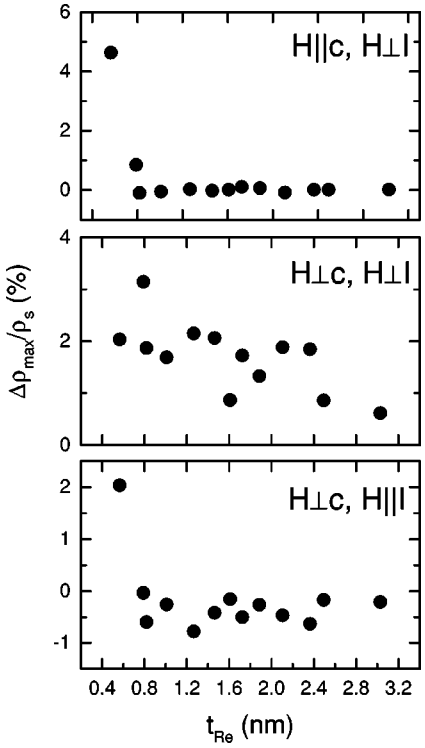

FIG. 14. The MR measured with respect to saturation as a function of t_{Re} measured in three different configurations. H is the applied magnetic field, c is the c axis, and I is the applied current.

situation where the surface spin-flop nucleates a gradual transition in the bulk, as discussed above. We also note that the large anisotropy value makes the Folkerts calculation barely applicable, since in this case $J_{\mathrm{AF}}/2K_U t_{\mathrm{Co}}=1.04$. This could also be a result of lateral disorder, which would cause a distribution in exchange constants, or different anisotropy constants at the top and bottom Co layers, which would smear out the surface spin-flop transition.

We can qualitatively analyze the magnetoresistance in the three other configurations in Fig. 9 by again taking into account the GMR, the AMR, and the spin-flop transition. For the $H\|c$, $H\|I$ case [Fig. 9(b)], as the field is lowered from its maximum value, the angle between the Co layer magnetizations in spin-flop increases. This causes M to have a component perpendicular to I, so that the AMR decreases the resistivity. As the field is decreased even further and adjacent Co layers become antiferromagnetically aligned $\|c$, the resistivity increases due to both the GMR and the AMR. For the $H\perp c$, $H\perp I$ case [Fig. 9(c)], there is no spin-flop transition and the magnetization continuously goes from a parallel alignment to an antiparallel alignment as the field is lowered to zero. According to Folkerts,[31] the GMR is always negative in this case with little or no hysteresis. The AMR is also negative since $M\perp I$ at saturation and $M\|I$ near $H=0$. Therefore, a relatively large MR is observed (3.3%). The $H\perp c$, $H\|I$ case [Fig. 9(d)] is the same as the previous case, except that the initial drop in the MR is due to the AMR since in this case $M\|I$ at saturation and $M\perp I$ near $H=0$, whereas the increase in MR near $H=0$ is due to the GMR. The two effects are almost of equal magnitude in this configuration, so the net change in MR from saturation to $H=0$ is approximately zero.

The results for the $t_{\mathrm{Re}}=0.79$ nm sample can be compared with those of the $t_{\mathrm{Re}}=1.46$ nm sample in Fig. 10. For the $H\|c$, $H\perp I$ case [Fig. 10(a)] the MR is very small. If the Co layers are magnetically uncoupled, there is essentially no change in the orientation of M as the field is lowered, until both magnetizations flip at a negative field. Therefore, M is always $\perp I$, and both the AMR and the GMR are zero. The small field dependence could be due to the normal magnetoresistance of the Re. For the $H\|c$, $H\|I$ case [Fig. 10(b)], the MR is also not expected to change for the same reasons. In practice, a small amount of negative MR ($\sim 0.1\%$) is observed, perhaps due to a slight misalignment of the sample with respect to the field. For the $H\perp c$, $H\perp I$ case [Fig. 10(c)], one would expect M to increasingly point along the easy axis as H is lowered from saturation. This causes an increase in the AMR, which is reflected in the $\sim 2\%$ negative MR shown in the figure. For the case of $H\|c$, $H\|I$ [Fig. 10(d)], one would expect the same behavior as in the previous case, but with a positive AMR, which is exactly what is observed in the figure.

The plausibility of our explanation of the unusual behavior of the $t_{\mathrm{Re}}=0.79$ nm sample can be analyzed using the orientation of the magnetic moments of the layers deduced from neutron reflectivity measurements.[22] A sketch of the magnetic moments of two adjacent Co layers, as deduced from the neutron reflectivity, is shown in Fig. 11 for the $H\|c$ case. Note the gradual spin-flop transition. The $M-H$ loop can be calculated from the sum of the components of $\vec{M}_1$ and $\vec{M}_2$ along H, where $\vec{M}_1$ and $\vec{M}_2$ are the magnetizations in adjacent Co layers. To simulate the MR, expressions are needed for the AMR and the GMR. The GMR is proportional to the magnitude of the net antiferromagnetic moment in the sample, or

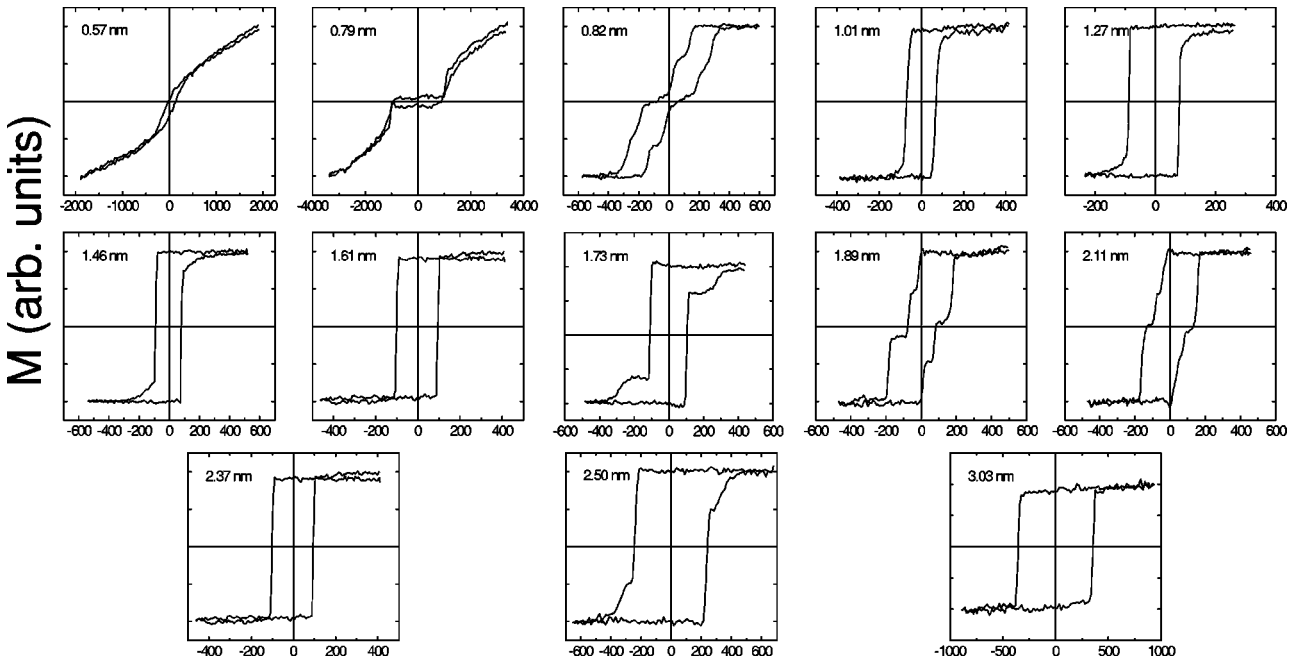

FIG. 15. MOKE magnetization loops measured with H applied parallel to the easy axis. The Re thickness is indicated in each figure.

$$\frac{\Delta\rho_{\mathrm{GMR}}}{\rho_{\mathrm{sat}}} = A\frac{|\vec{M}_1(H)-\vec{M}_2(H)|}{|\vec{M}_1(0)-\vec{M}_2(0)|}, \tag{6}$$

where A is a constant, $\vec{M}(H)$ is the magnetization of adjacent Co layers as a function of applied magnetic field H, and ρ_{sat} is the resistivity at saturation. The AMR depends on the components of the magnetization parallel and perpendicular to the applied current. The total AMR contribution to the resistivity can be written as

$$\frac{\rho_{\mathrm{AMR}}-\rho_{\perp}}{\rho_{\parallel}-\rho_{\perp}} = \frac{1}{2}(\cos^2\gamma_1+\cos^2\gamma_2), \tag{7}$$

where γ_1 and γ_2 are the angles of the magnetization of two adjacent Co layers with respect to the applied current. Note that in the AMR, for $H\|I$, $\rho_{\mathrm{sat}}=\rho_{\parallel}$, and for $H\perp I$, $\rho_{\mathrm{sat}}=\rho_{\perp}$.

Figure 12 shows the calculated magnetoresistance in the same current and field configurations used in the experiments. The only adjustable parameters are A for the GMR, and $\Delta\rho$ for the AMR. The results of this simple phenomenological model reproduce the qualitative features of the data in Fig. 9 except for the $H\perp c$, $H\|I$ case. The poor agreement in this case may result from not accounting for the possibility of misaligning the c axis with the applied field or contributions due to a more complicated domain structure not taken into account by the model. Note that in this case the contribution to the MR is roughly an order of magnitude smaller than in the other configurations, which makes it vulnerable to other second order effects not taken into account by the model.

For a comparison of the MR and magnetization data, the calculated MR and $M-H$ loop for the $H\|c$, $H\perp I$ case is plotted in Fig. 13. *Notice that in the simulation, as in the actual data, the switching field does not correspond to the peak in the MR.* From a qualitative analysis of MR measurements we conclude that the Co layers in the $t_{\mathrm{Re}}=0.79$ nm are coupled antiferromagnetically. We note that the MR of the $t_{\mathrm{Re}}=0.57$ nm sample behaves like the $t_{\mathrm{Re}}=0.79$ nm sample in that the $H\|c$, $H\perp I$ MR also shows a dip near $H=0$ and that the magnitude of the MR is substantial.

In order to obtain further insight into the magnetic coupling, Fig. 14 shows the MR, $\Delta\rho_{\mathrm{max}}/\rho_s \equiv (R(0)-R(30\ \mathrm{kOe}))/R(30\ \mathrm{kOe})$, where $R(H)$ is the electrical resistance as a function of magnetic field. In the $H\|c$, $H\perp I$ configuration, the MR drops precipitously as t_{Re} increases. Although it is tempting to conclude that the antiferromagnetic coupling is small or zero for $t_{\mathrm{Re}}>1.0$ nm, other types of measurements must also be performed to prove this. The reason is that if $|J_{\mathrm{AF}}|<K_U t_{\mathrm{Co}}$, only a very small GMR and AMR would be observed because the magnetizations of adjacent Co layers would not undergo a spin-flop transition.[31] Since K_U increases with t_{Re}, the GMR would be reduced if J_{AF} did not increase with t_{Re}. An indication that this is the case for the Co/Re samples is the MR behavior in the $H\perp c$, $H\perp I$ configuration. In this case, there should always be a GMR[31] and the AMR should always be negative (the same sign as the GMR). In Fig. 14(b) the value of $\Delta\rho/\rho$ decreases, but seems to oscillate slightly as t_{Re} increases, which is reminiscent of the GMR oscillations in the Co/Ru and Co/Cr systems.[3] In this configuration, however, it is impossible to determine whether the GMR or the AMR oscillate. Nevertheless, the possible peaks in the $H\perp c$, $H\perp I$ configuration correspond to dips in the $H\perp c$, $H\|I$ configuration. We therefore conclude that the nonmonotonic variations in the MR for $t_{\mathrm{Re}}>1.0$ nm are a result of variations in the AMR of the samples, because the GMR should have the same sign, irrespective of the direction of the applied current. The variations could be due to small differences in the structure or Co layer thickness.

The behavior of the magnetization hysteresis loops measured with $H\|c$ shown in Fig. 15, however, could be an indication that AF coupling could also occur for $t_{\mathrm{Re}}\sim 2.0$ nm samples, because their hysteresis loops are sheared

or have steps. A similar behavior has been observed in Fe/Cr(211) superlattices.[7] The lack of a significant GMR for the $t_{Re} \sim 2.0$ nm samples could be due to a weakening J_{AF}, combined with a larger K_U as discussed above. However, the steps in the magnetization loops could also be caused by the formation of complex domain structures, so additional experimental evidence, such as neutron reflectivity measurements, is needed to prove this hypothesis.

IV. SUMMARY AND CONCLUSIONS

We have grown epitaxial hcp Co/Re$(10\bar{1}0)$ superlattices on $Al_2O_3(11\bar{2}0)$ substrates. The interfaces of the samples were quantitatively analyzed using low angle x-ray reflectivity. The results show that ~ 0.4 nm of material, or two monolayers of each material are mixed at each of the interfaces. High angle x-ray diffraction, including in-plane ϕ scans, show that the films are epitaxial. The magnetization of the samples measured via SQUID magnetometry agree with the FMR effective magnetization to within the uncertainty of the data, which indicates that there is no significant out-of-plane magnetic anisotropy. Because the c axis of these samples is in the plane, a significant in-plane magnetic anisotropy is observed. The in-plane uniaxial anisotropy constants K_1 and K_2 were also determined from FMR measurements. For thicker Re samples ($t_{Re} > 1.0$ nm), $K_1 \sim 0.7 \times 10^6$ erg/cm^3 and $K_2 \sim 0.2 \times 10^6$ erg/cm^3. These values are approximately 5 times lower than in bulk Co, but the ratio of these two numbers is the same as that observed in thick Co films. This could be a result of the crystalline strain in the Co layers. For thin Re samples ($t_{Re} < 1.0$ nm), magnetoresistance measurements clearly indicate the presence of GMR, due to antiferromagnetic coupling between the Co layers, as was previously observed in (0001)-oriented Co/Re multilayers.[5] In these samples the MR behavior is relatively complex due to the spin-flop transition which results in a competition between the GMR and AMR effects. Magnetization hysteresis loops also suggest that antiferromagnetic coupling may be present at other Re thicknesses, although further studies are necessary to unequivocally prove this. We conclude that the GMR in Co/Re superlattices for thicker Re layers is not necessarily due to a lack of antiferromagnetic coupling, but could be a result of the large magnetic anisotropy of the Co layers with respect to the antiferromagnetic coupling between the Co layers. These results show that in Co-based multilayers with a strong in-plane anisotropy it is important to take into account the AMR as well as the GMR. Together, these two effects could be used to significantly enhance the efficiency of magnetoresistance-based devices.

ACKNOWLEDGMENTS

We thank E. Mayo for performing some of the x-ray measurements, M. Koepke for providing the Re sputtering target, and D. Windt and E. E. Fullerton for useful discussions. This research was supported by the Petroleum Research Fund (Grant ACS-PRF No. 32814-G5) and the U.S. National Science Foundation (Grant No. DMR-9734051) at WVU, and the U.S. Department of Energy (Grant No. DE-FG02-86ER45281) at MU.

[1] M. N. Baibich, J. M. Broto, A. Fert, F. Nguyen Van Dau, F. Petroff, P. Etienne, G. Creuzet, A. Friederich, and J. Chazelas, Phys. Rev. Lett. **61**, 2472 (1988).

[2] P. Grünberg, R. Schreiber, Y. Pang, M. B. Brodsky, and H. Sowers, Phys. Rev. Lett. **57**, 2442 (1986).

[3] S. S. P. Parkin, N. More, and K. P. Roche, Phys. Rev. Lett. **64**, 2304 (1990).

[4] For a review, see A. Fert, P. Grünberg, A. Barthélémy, F. Petroff, and W. Zinn, J. Magn. Magn. Mater. **140-144**, 1 (1995).

[5] P. P. Freitas, L. V. Melo, I. Trindade, M. From, J. Ferreira, and P. Monteiro, Phys. Rev. B **45**, 2495 (1992).

[6] L. V. Melo, I. Trinidade, M. From, P. P. Freitas, N. Teixeira, M. F. da Silva, and J. C. Soares, J. Appl. Phys. **70**, 7370 (1991).

[7] E. E. Fullerton, M. J. Conover, J. E. Mattson, C. H. Sowers, and S. D. Bader, Phys. Rev. B **48**, 15 755 (1993).

[8] J. C. A. Huang, Y. Liou, Y. D. Yao, W. T. Yang, C. P. Chang, S. Y. Liao, and Y. M. Hu, Phys. Rev. B **52**, R13 110 (1995).

[9] Th. Zeidler, K. Theis-Bröhl, and H. Zabel, J. Magn. Magn. Mater. **187**, 1 (1998).

[10] J. J. Picconatto, M. J. Pechan, and E. E. Fullerton, J. Appl. Phys. **81**, 5058 (1997).

[11] G. R. Harp and S. S. P. Parkin, Appl. Phys. Lett. **65**, 3063 (1994).

[12] H. Yanigihara, K. Pettit, M. B. Salamon, E. Kita, and S. S. P. Parkin, J. Appl. Phys. **81**, 5197 (1997).

[13] R. W. Wang, D. L. Mills, E. E. Fullerton, J. E. Mattson, and S. D. Bader, Phys. Rev. Lett. **72**, 920 (1994).

[14] S. K. Sinha, E. B. Sirota, S. Garoff, and H. B. Stanley, Phys. Rev. B **38**, 2297 (1988).

[15] B. Vidal and P. Vincent, Appl. Opt. **23**, 1794 (1984).

[16] M. A. Tomaz, G. R. Harp, E. Mayo, D. Lederman, R. Wu, and W. L. O'Brien, J. Vac. Sci. Technol. A **16**, 1336 (1998).

[17] M. M. Schwickert, R. Coehoorn, M. A. Tomaz, E. Mayo, D. Lederman, W. L. O'Brien, T. Lin, and G. R. Harp, Phys. Rev. B **57**, 13 681 (1998).

[18] For a review of MOKE in thin films, see S. D. Bader and J. L. Erskine, in *Ultrathiin Magnetic Structures II*, edited by B. Heinrich and J. A. C. Bland (Springer-Verlag, Berlin, 1994), p. 297.

[19] F. Schreiber, Z. Frait, Th. Zeidler, N. Metoki, W. Donner, H. Zabel, and J. Plezl, Phys. Rev. B **51**, 2920 (1995).

[20] *Binary Alloy Phase Diagrams* (ASM International, Materials Park, OH, 1990), p. 1229.

[21] E. E. Fullerton, I. K. Schuller, H. Vanderstraeten, and Y. Bruynseraede, Phys. Rev. B **45**, 9292 (1992).

[22] T. Charlton, D. Lederman, S. M. Yusuf, and G. Felcher, J. Appl. Phys. (to be published).

[23] C. A. Ramos, D. Lederman, A. R. King, and V. Jaccarino, Phys. Rev. Lett. **65**, 2913 (1990).

[24] S. Chikazumi, *Physics of Magnetism* (Wiley, New York, 1964), p. 129.

[25] J. Z. Hilt, J. J. Picconatto, A. O'Brien, M. J. Pechan, and E. E. Fullerton, J. Magn. Magn. Mater. (to be published).

[26] M. Grimsditch, E. E. Fullerton, and R. L. Stamps, Phys. Rev. B **56**, 2617 (1997).
[27] J. Smit, Physica (Amsterdam) **16**, 612 (1951).
[28] For a review, see I. A. Campbell and A. Fert, in *Ferromagnetic Materials*, edited by E. P. Wohlfarth (North-Holland, Amsterdam, 1982).
[29] P. P. Freitas, A. A. Gomes, T. R. McGuire, and T. S. Plaskett, J. Magn. Magn. Mater. **83**, 113 (1990).
[30] C. Kittel, *Introduction to Solid State Physics*, 6th ed. (Wiley, New York, 1986), p. 144.
[31] W. Folkerts, J. Magn. Magn. Mater. **94**, 302 (1991).